J. Webster (ed.), *Wiley Encyclopedia of Electrical and Electronics Engineering*

HIGH-T_c SUPERCONDUCTORS, PHYSICAL STRUCTURES, AND ROLE OF CONSTITUENTS

Since the discovery of the phenomenon of superconductivity in 1911 by H. Kamerlingh Onnes (1), superconductors have been a topic of great interest from fundamental as well as application points of view. With the discovery of high-temperature superconductors (*HTSCs*) in 1986 (2), the field of superconductivity achieved even greater interest. Since then HTSCs have moved into the realm of practical applications because they are mostly superconducting above the boiling point of liquid nitrogen (77 K), which is cheaper than and has a much greater cooling capacity than liquid helium. Therefore, for any application in which liquid nitrogen can replace liquid helium, the refrigeration cost for operating superconductive devices will be about 1000 times less.

The newly discovered HTSCs are copper-oxide–based ceramics that remain superconducting near 100 K. This temperature regime does not seem high, but it is high enough for liquid nitrogen to cool most of HTSCs into the superconducting range. For example, the compound yttrium barium copper oxide (YBCO) has been found to be superconducting up to 92 K (3). Additional important high-temperature superconductors include bismuth strontium calcium copper oxide (*BSCCO*) (4), thallium barium calcium copper oxide (*TBCCO*) (5), and mercury barium calcium copper oxide (*HBCCO*) (6). HBCCO has the highest critical temperature, $T_c = 135$ K (7,8). Table 1 presents the chemical formula and T_c values of each of these compounds. The HTSCs can be subdivided into three classes: three-dimensional compounds based on $BaBiO_3$, layered copper-oxide compounds with hole conductivity (based on La_2CuO_4, $YBa_2Cu_3O_{7-}$, and compounds of Bi and Tl), and compounds based on Nd_2CuO_4 with electron conductivity. With increasing number of CuO_2 planes in copper-oxide superconductors, a certain increase in T_c is observed. Its values range from $T_c = 36$ K in $La_{2-x}Sr_xCuO_4$ with a single CuO_2 plane to $T_c = 125$ K in compounds of Tl (2223) with three CuO_2 planes.

Common Features of High-T_c Superconductors

Coherence Length and London Penetration Depth. In addition to the crystallographic aspects of the HTSC oxides, there are more fundamental parameters contributing to the anisotropic nature of these materials. Central to the theory of superconductivity is the Cooper electron pair discovered by Cooper in 1956 (9), when he showed that it is possible for electrons to have an attractive interaction leading to a lowering of energy of the system. One result of the pairing is that electric current can flow without resistance, giving rise to superconductivity. The critical temperature is related to the thermal energy required to destroy the pairing between the paired electrons. Earlier in 1950, Ginzberg and Landau showed that the spatial variation of the particle or superelectrons carrying the resistanceless current can be described by the coherence length ξ. The parameter ξ gives the length scale for the density variation of Cooper pairs, and simply put, the greater the length, the larger the hurdle the pairs can cross without breaking up. The breaking of pairs means the destruction of superconductivity, and so care must be taken to keep the material free of features that break these pairs. The other important length in superconductivity is the London penetration depth λ_L, which sets the scale for the decay of an external magnetic field as a function of depth in the superconducting material.

Table 1. List of Common High-T_c Superconductors

Name	Formula	T_c (K)
Yttrium barium copper oxide	$Y_1Ba_2Cu_3O_7$	90
Bismuth strontium calcium copper oxide	$(Bi, Pb)_2Sr_2Ca_2Cu_3O_x$	105
Thallium barium calcium copper oxide	$Tl_1Ba_2Ca_2Cu_3O_x$	115
Mercury barium calcium copper oxide	$Hg_1Ba_2Ca_2Cu_3O_x$	135

There is a strong parallel between the skin depth of metals in response to high-frequency fields and the London depth in response to magnetic fields. In 1935, the London brothers first introduced the concept of penetration depth while following a phenomenological approach to superconductivity via Maxwell's equations for electromagnetism (10).

Ginzberg and Landau (*GL*) showed that the ratio of $\kappa = \xi/\lambda_L$ determined the nature of the response of the superconductor to a magnetic field. For $\kappa \leq 1/2$, type-I superconductivity exists, and there exists a critical field H_c when superconductivity and diamagnetism are abruptly destroyed, while for $\kappa \geq 1/\sqrt{2}$, type-II superconductivity exists, and there exists a lower critical field H_{c1} above which materials are not perfectly diamagnetic and an upper critical field H_{c2} beyond which superconductivity and diamagnetism are completely destroyed. All the HTSC oxide superconductors are type II and are potentially useful because they can sustain high magnetic fields and remain superconducting.

Anisotropy. In addition to the crystallographic anisotropy, there are a number of important properties that also show anisotropy such as electrical conductivity, thermal conductivity, magnetic field penetration, and current density. The large variation in electrical and thermal conductivity in directions parallel to and perpendicular to the *c* axis is a direct consequence of the conductivity of the CuO_2 layers. Ratios of 100 and 17 for the electrical and thermal conductivities parallel to the *a*–*b* plane and perpendicular to it have been measured for YBCO (11). These values are even higher in Bi- and Tl-based systems, indicating strong anisotropy parallel to and perpendicular to the CuO_2 layers. Anisotropy in response to magnetic fields and current density is a result of the large variation in the coherence length with direction. For YBCO, ξ is a few nanometers along the *a*–*b* plane and an order of magnitude less perpendicular to it. This produces a large variation in the magnetic field and current density it can support perpendicular to and parallel to the *a*–*b* plane. Similar features are observed in the other HTSC systems.

Structures of High-T_c Superconductors

The knowledge of structure is a prerequisite for understanding the properties of high-T_c superconductors. The structures of high-T_c superconductors can be easily analyzed by considering the structure of a perovskite. The original mineral called perovskite was $CaTiO_3$ and was described in the early nineteenth century by Gustav Rose. In addition to the importance of perovskite structures in superconductivity, dielectric, piezoelectric, pyroelectric, and ferroelectric properties of compounds with perovskite structures have found widespread applications in memory devices, capacitors, tunable filters, microphones, loudspeakers, etc.

The chemical formula for a perovskite structure is ABX_3, where *A* and *B* are metal cations and *X* is a nonmetal anion. *X* is either oxygen (*O*) or a member of the halogen family, such as fluorine, bromine, or chlorine. The perovskite cell consists of a relatively large metallic atom (*A*) at the corners (or center), smaller metallic atoms (*B*) at the center (or corners), and the nonmetallic atom (*X*) at face centers (or midpoint between the

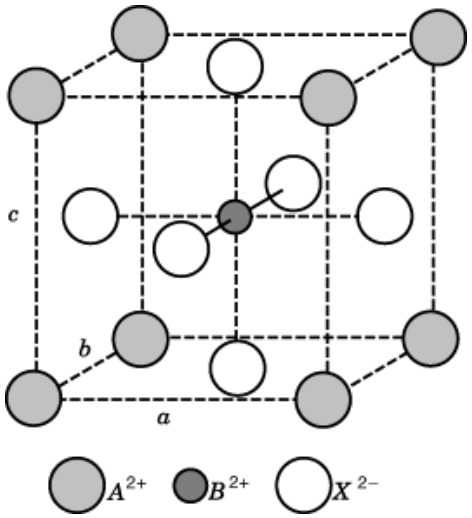

Fig. 1. A schematic representation of a perovskite structure.

corners). Figure 1 illustrates the position of the various atoms on a cube. The chemical formula of ABX_3 is easily deduced from this figure if the eight unit cells sharing the corner A atom and the two unit cells sharing the X atoms are considered. The atom positions can be designated as A: (0,0,0) corner sites; X: $(0,\frac{1}{2},\frac{1}{2})$, $(1,\frac{1}{2},\frac{1}{2})$; $(\frac{1}{2},\frac{1}{2},0)$, $(\frac{1}{2},\frac{1}{2},1)$; $(\frac{1}{2},0,\frac{1}{2})$, $(\frac{1}{2},1,\frac{1}{2})$ edge centers;B: $(\frac{1}{2},\frac{1}{2},\frac{1}{2})$ body center.

Another representation of the perovskite structure that is extremely useful to the understanding of HTSC oxide structures is the layered or planar approach in which the structure is formed by stacking of layers in the z direction. In this approach, the molecular grouping comprising each layer is also shown mainly in order to stress the importance of the layered approach to an understanding of the properties of the HTSC oxides. The layers themselves usually do not have any significance and may not even exist as independent structures. In HTSC oxide terminology, the long axis is denoted by c (or z) as compared to the smaller a or b axis.

An ideal perovskite is cubic, like $CaTiO_3$. Its strong ionic bonding makes $CaTiO_3$ electrically insulating and a hard mineral. It also shows three-dimensional isotropy in many properties due to the cubic symmetry. The crystallographic nature of anisotropy or isotropy does not necessarily determine the nature of fundamental properties of materials such as its electrical conductivity. For instance, the element gallium exists as an anisotropic hexagonal structure, but the momentum distribution of its electrons termed *momentum space* is isotropic, and similar features could occur for superconductors. In general, there are a number of variations from the ideal form of $CaTiO_3$. A typical example is the diversity in properties demonstrated by $BaTiO_3$. The crystal structure of $BaTiO_3$ undergoes structural phase transitions as a function of the ambient temperature, changing its symmetry and response to external electric fields. Below 5°C it has an orthorhombic structure, between 5°C and 210°C it is tetragonal, while above 210°C it is cubic. In the tetragonal state, the structural distortion results in a permanent electric dipole moment, making it ferroelectric, while in the cubic phase the symmetry prevents the existence of a permanent dipole moment. In noncubic perovskite minerals the phenomenon of twinning is commonly observed. Twinning is most easily described by considering a structure obtained by interchanging the a and b axis in a tetragonal phase, resulting in regions that are mirror images of each other.

In addition to these common structural features, the role of the A and B cations is also crucial in the properties of perovskites. The replacement of the smaller Ca^{2+} with an ionic radius of 0.99 Å with the larger Ba^{2+} (1.34 Å) plays a central role in the tetragonal distortion leading to the ferroelectric property of $BaTiO_3$. The

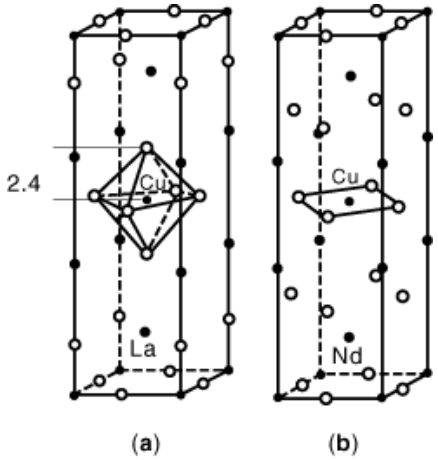

Fig. 2. Comparison of structures of La- and Nd-based superconductors. (a) Structure of La_{2-x} Ba_xCuO_4 with sixfold-coordinated Cu. This is a *p*-type superconductor. (b) Structure of Nd_2CuO_4 with planar fourfold-coordinated Cu. When some Nd^{3+} ions are replaced by Ce^{4+}, this material becomes an *n*-type superconductor.

doping or substitution of *A* or *B* cations with other ions having radii within 15%, but with different valence, results in a charge imbalance that is compensated by the creation of holes or equivalently by vacancies in the *X* sites. This charge imbalance results in nonstoichiometric perovskite structures. All the HTSC oxide superconductors contain Cu^{2+} instead of Ti^{4+}, resulting in a CuO_2 layer that plays a central role in the nature of electric current transport in these materials. Because of this feature all the HTSC oxides exhibit an almost uniform size of *a* and *b* axes (usually between 3.81 Å and 3.83 Å). In addition to these aspects, structural transformations, twinning, anisotropy, etc., are all key features in controlling the superconducting properties and need to be studied in detail to obtain a clearer picture of the behavior of these complex and potentially useful structures.

Structure of La–(Ba,Sr,Ca)–Cu–O and Nd(Ce)–CuO Compounds. Superconductivity in the high-T_c oxides was first discovered in the La_2CuO_4 system when Bednorz and Muller 2 observed a sharp drop in the electric resistance in Ba-doped $La_{2-x}Ba_xCuO_4$. Subsequent observation of the Meissner effect confirmed that the compound was superconducting. The T_c was maximized at 30 K for a value of $x = 0.15$. The structure of the superconducting phase was identified as a derivative of the layered perovskite K_2NiF_4 and is shown in Fig. 2. The CuO_2 layers consist of octahedrally coordinated Cu, with the Cu–O bond length of 1.9 Å in the *a*–*b* plane and 2.4 Å in the *c* direction. Also, the Cu atoms occur at (000) and ($\frac{1}{2}$ $\frac{1}{2}$ $\frac{1}{2}x^4$,) lattice sites in the unit cell, similar to a body-centered structure. The substituted Ba^{2+} ions occupy a fraction of the La^{3+} sites, and the difference in valence brings about an increase in the number of holes. Superconductors with hole conduction are called *p* type, a terminology similar to that followed in semiconductors. While substitution with atoms of different valence is a well-known technique to introduce excess holes or electrons (once again in parallel with semiconductors), oxidation or reduction to change the oxygen content also changes carrier concentration. Interstitial oxygen between the LaO sheets or missing oxygen from the lattice sites, that is, vacancies, can also lead to excess charge carriers. For example, the electrochemical oxidation of La_2CuO_4 results in *p*-type superconductivity (12). Substitution of the smaller (1.12 Å)Sr^{2+} ions instead of Ba^{2+} (1.34 Å) results in a higher T_c (39 K) for $x = 0.15$. The increase in T_c by substitution of a smaller atom and also the fact that increasing pressure tends to increase T_c [i.e., in the $La_{1.8}Ba_{0.2}CuO_4$ phase, T_c increases from 31 K to 36 K for a pressure increase from atmosphere to 1.2 GPa (13)] is a significant property for a fundamental understanding of high-temperature superconductivity and it also points the way to the synthesis of oxide superconductors with higher T_c.

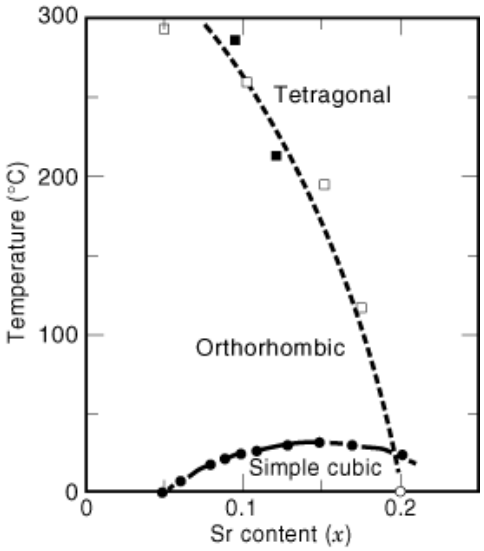

Fig. 3. Structural phase changes in La-based copper oxides as function of Sr concentration. (Adapted from Ref. 15.)

The structure of compounds in the Nd_2CuO_4 system is identical to the compounds in the La-based copper oxides. The only difference arises in the positions of the oxygen atoms, giving rise to an O_2 layer instead of the La–O layer present in La-based structures. While this does not change the CuO_2 layers, it results in a square planar fourfold copper coordination as seen in Fig. 2, which compares the structures of the La- and Nd-based superconductors. The most important feature of Nd-based materials derives from the fact that superconductivity in this system is by electroconduction or *n*-type rather than hole conduction as in La-based superconductors. The difference in conductivity between the two systems, which in the undoped state have almost identical structures and trivalent lanthanum or neodymium, is owing to the effect of doping the substituting La with divalent Sr and the Nd with tetravalent Ce. In one case it results in a decrease in the number of electrons ($La^{3+} + e^- \rightarrow Sr^{2+}$), leading to excess holes, while in the other it increases the number of electrons ($Nd^{3+} + h^+ \rightarrow Ce^{4+}$), leading to *n*-type conductivity. The electroconducting compound $Nd_{1.85}Ce_{0.15}CuO_{4-\delta}$ with $T_c = 24$ K is the most studied material in this system (14).

Another common feature observed among the HTSC oxide families is easily observed in $La_{2-x}(B = Ba, Sr)_xCuO_4$. Here, the lattice parameters and crystallographic symmetry depend on the value of x. For $x = 0.2$ and $B = Sr$, the structure is tetragonal, while it is orthorhombic for $x < 0.2$. Figure 3 shows the structural phase diagram for the $La_{2-x}Sr_xCuO_4$ system (15). Similar features can be found for $B = Ba$. One aspect of the structures in La-based compounds is that superconductivity is observed both in the orthorhombic and tetragonal phase, a feature not seen in the Y–Ba–Cu–O system, where only the orthorhombic phase superconducts.

Y–Ba–Cu–O Compounds. The increase in T_c observed by increasing pressure and by substitution of smaller atoms led Chu and his co-workers (13) to replace La^{3+} (ionic radius of 1.14 Å) by the smaller Y^{3+} (0.94 Å), leading to the first superconductor with a transition temperature (T_c) higher than the boiling point of liquid N_2 (77 K). The compound synthesized was $YBa_2Cu_3O_{7-\delta}$ with a T_c of 92 K. $YBa_2Cu_3O_{7-\delta}$ is also commonly referred to in the literature as Y123 or generally as YBCO and is the most widely studied of all the HTSC oxides. Its superconducting properties, such as T_c, the maximum current that it can carry (measured by the current flowing per unit cross-section area of the superconducting material, i.e., the critical current density, J_c), and the maximum strength of magnetic field that it could expel via the Meissner effect (H_c), are all highly sensitive to the crystal structure and crystal quality of the YBCO material.

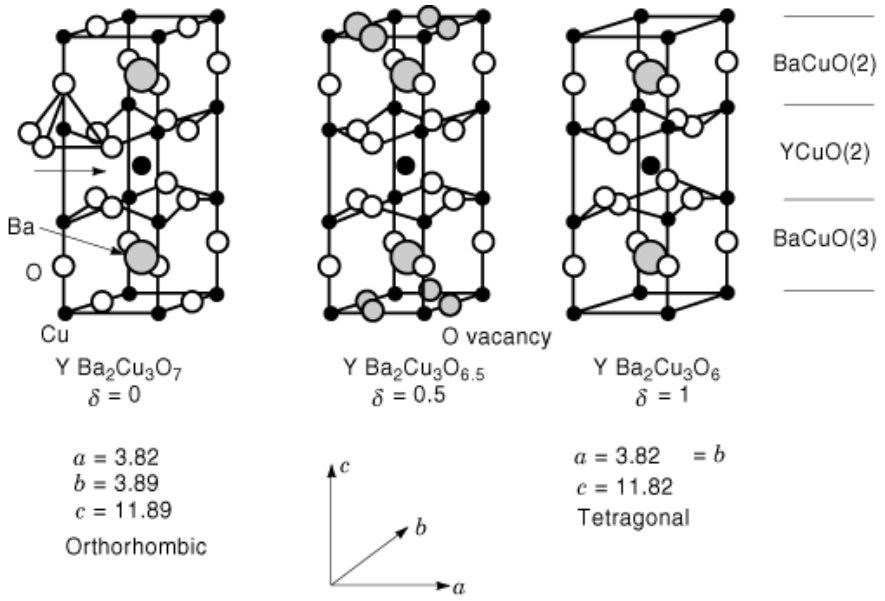

Fig. 4. Structure of $Y_1Ba_2Cu_3O_{7-\delta}$. The oxygen content (δ) varies from 1 (rightmost figure) to 0 (leftmost figure) changing the structure from a tetragonal insulating phase to the superconducting orthorhombic YBCO phase. The fivefold coordination of the Cu in the copper oxide plane is also shown. The chain oxygen content (in the a–b plane) varies with δ. The distortion of the CuO_2 planes is also seen.

In terms of the perovskite structure, $YBa_2Cu_3O_{7-\delta}$ is modeled by stacking three perovskite-type cells of type $BaCuO_3$, $YCuO_2$, and $BaCuO_2$ as shown in Fig. 4. A BaO plane separates two layers containing Cu and O. While one contains atoms in the ratio of 1:2, that is, CuO_2, the other contains a varying quantity of O, ranging from CuO to Cu. The two layers are commonly referred to as the CuO_2 plane or CuO chain, respectively. The quantity of oxygen in the chains is the key to properties of $YBa_2Cu_3O_{7-\delta}$ and is represented by the value of δ, known as the oxygenation parameter. For $\delta = 1$, the chains do not contain O (Fig. 4), while for $\delta = 0$, the chains are fully oxygenated, giving a CuO layer. The δ value also determines the crystal structure of YBCO, and Fig. 4 (left to right) shows the transition from an orthorhombic structure ($a = 3.82$ Å, $b = 3.89$ Å, $c = 11.68$ Å) for $\delta = 0$ to a tetragonal structure for $\delta = 1$ ($a = b = 3.86$ Å, $c = 11.82$ Å). Significantly, in the tetragonal phase obtained for $\delta \geq 0.6$, the material is insulating and does not have a superconducting transition, while in the orthorhombic state obtained for $\delta \leq 0.6$, it is metallic and superconducting. T_c is seen to maximize at 92 K as δ approaches zero. δ can be measured either using the titration method or from the lattice parameter of YBCO obtained from X-ray diffraction (XRD) measurements using an empirical formula, $\delta = (c - 11.68)/0.1501$, suggested by Tranquada et al. (16). Here, c is the value of the c parameter obtained from XRD measurements. Figure 5 shows the experimentally observed correlation between the c-axis lattice parameter and T_c for YBCO in both thin-film form (17) and bulk form (18). The higher values of the c-axis lattice parameter for YBCO thin film than those for bulk YBCO with the same T_c are attributed to the expansion of the unit cell under the influence of the substrate material.

In many cases, it is easier to interpret the properties of the HTSC oxides by understanding the stacking sequence of the individual Cu–O layers making up the unit cell. But, unlike the case of true layered compounds such as graphite and mica, where the weak bonds between layers makes intercalation with foreign atoms easy, this is not the case with the HTSC oxides, and so the layers must not be interpreted as such. In the case of the Bi-based HTSC oxides, though, the binding between BiO sheets is weak and intercalation of iodine is possible. Figures 6(a) and 6(b) compare the layering sequences in YBCO and La_2CuO_4. The main difference seems to

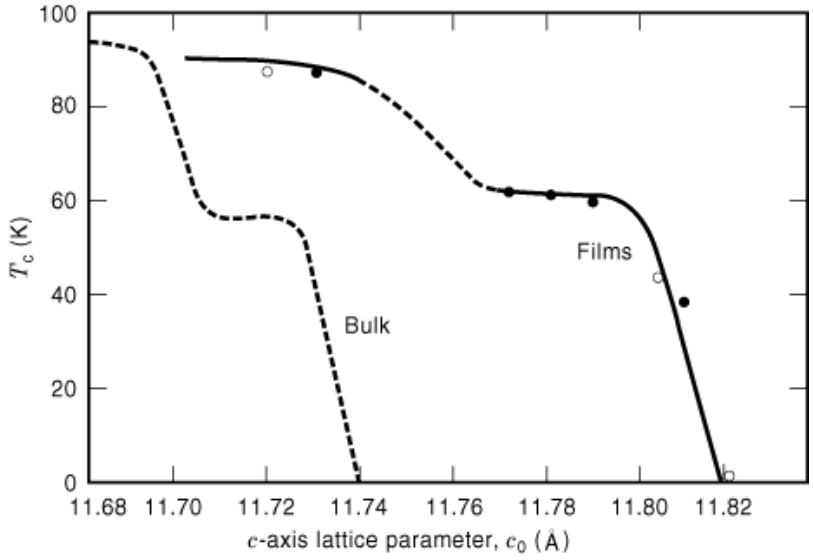

Fig. 5. Experimental correlation between the c-axis lattice parameter and T_c for YBCO thin film form (14) and YBCO bulk form. (Adapted from Ref. 18.)

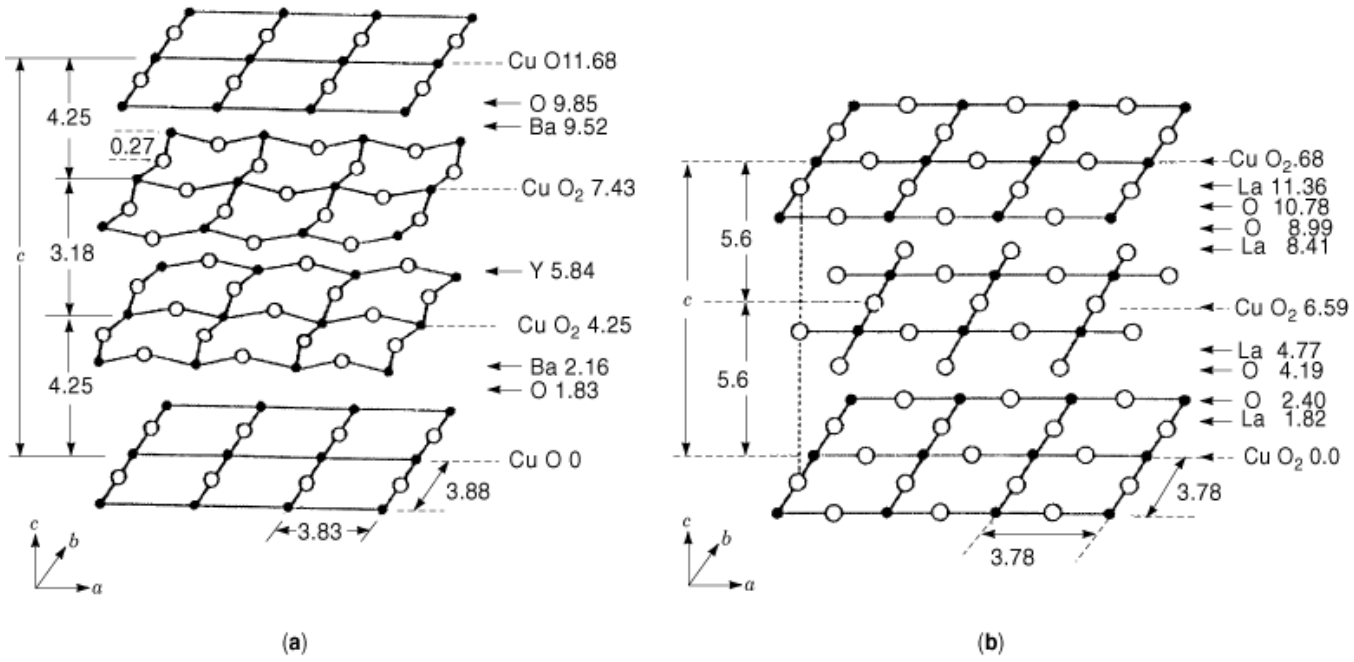

Fig. 6. Layered approach to the structure of copper oxide superconductors. (a) The $Y_1Ba_2Cu_3O_{7-\delta}$ structure with the individual planes and plane spacings in the c direction marked. (b) Similar approach for the La-based superconductors. (Adapted from C. P. Poole, H. A. Farach and R. J. Creswick, in *Su*, San Diego, CA: Academic 1995, pp. 182–191.)

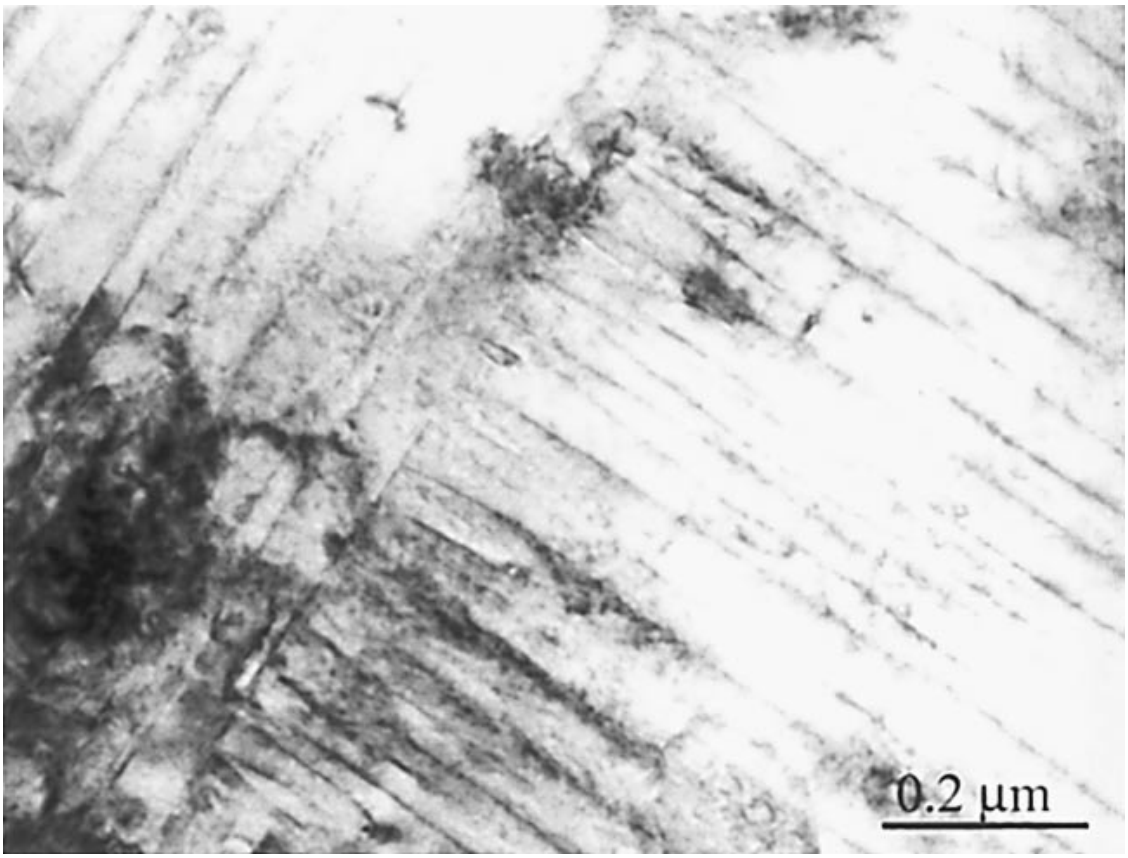

Fig. 7. Twinning in $Y_1Ba_2Cu_3O_{7-\delta}$. The figure shows a transmission electron microscope (TEM) image of a YBCO film grown on MgO by pulsed laser deposition. The striations correspond to the twin boundaries.

be in the form of the position of the individual Cu atoms. For the case of YBCO, all the Cu atoms are of one type; that is, edge type or all centered (depending upon the representation), while for the La-based structure, they occupy (000) and $(\frac{1}{2}\ \frac{1}{2}\ \frac{1}{2})$ positions. The Y layer acts as a spacer for the two CuO_2 planes in YBCO. Also unlike the case of La–Sr–Cu–O, the atoms on the CuO_2 layer in YBCO do not all lie on the same plane, that is, their z values differ slightly and so they are actually CuO_2 sheets as compared with CuO_2 planes. This slight distortion is visible in Figs. 4 and 6(a). Heating YBCO through 350°C transforms the orthorhombic structure to the tetragonal phase owing to the loss of oxygen. This displacing transition is the reason for twinning and is usually seen when the strain accompanying the phase change cannot be completely released, as in the case of crystalline thin films deposited on substrates. Thus, YBCO thin films undergo twinning when grown at high temperatures and subsequently cooled through 350°C in an oxygen ambient. Figure 7 shows a typical YBCO film showing twinning observed under an electron microscope.

In addition to YBCO, the Y–Ba–Cu–O family also contains other phases of which $YBa_2Cu_4O_8$ (Y124) has a T_c of ~80 K and $Y_2Ba_4Cu_7O_{15-\delta}$ (Y247) has a T_c of ~55 K. These two phases are not observed under normal processing conditions and require extremely high oxygen pressures or the addition of alkali-metal compounds in air at normal pressures (19). The structure of Y124 is similar to that of YBCO with the addition of an extra CuO chain layer displaced with respect to the first by a lattice parameter of $b/2$ (where the b axis contains the oxygen of the chains). Y124 is orthorhombic with $a = 3.84$ Å, $b = 3.87$ Å, $c = 27.2$ Å. The structure of Y247

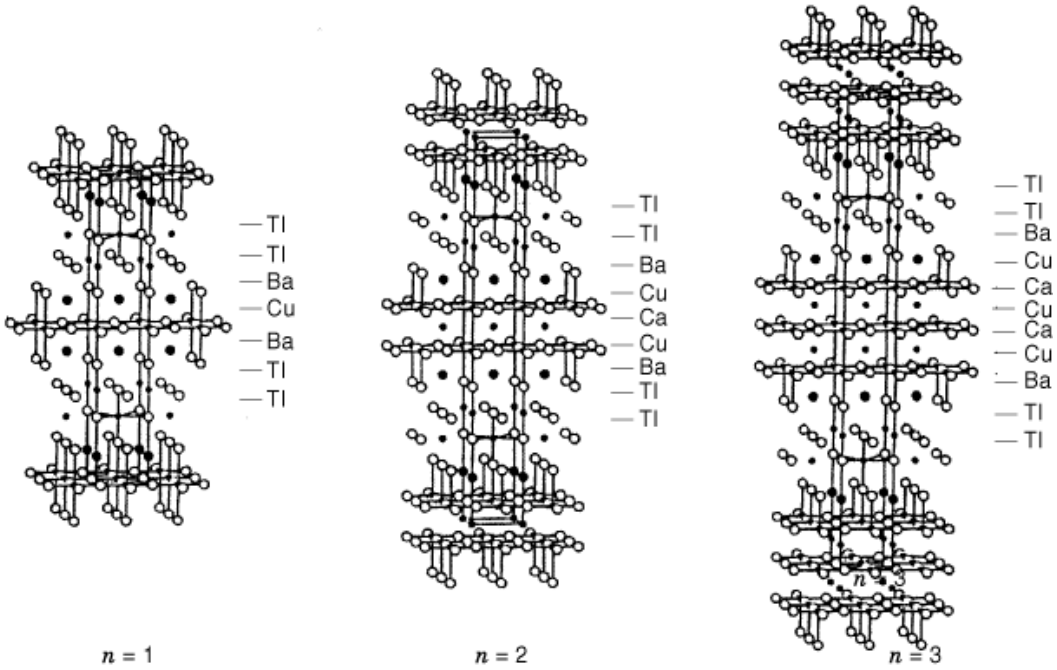

Fig. 8. Crystal structure of the Tl-(Bi-) based superconductors. Changing the number of Cu atoms introduces copper oxide layers (n). The structure of the Bi-based compounds is similar, with the Tl positions occupied by Bi. (Adapted from Ref. 21.)

can be represented by the intergrowth of alternating layers of YBCO and Y124, resulting in an orthorhombic structure of $a = 3.85$ Å, $b = 3.87$ Å, $c = 50.3$ Å. As compared to YBCO, Y124 has a fixed oxygen stoichiometry and so does not undergo the displacive transformation resulting in the twinning morphology.

Bi-, Tl-, and Hg-Based Compounds. In early 1988, two new superconducting systems based on bismuth and the toxic metal thallium with transition temperatures considerably higher than YBCO were discovered (20,21). These two systems have a and b lattice parameters similar to the Y- and La-based compounds, but with a much larger c parameter. The general formula for compounds occurring in this system is given by $A_2B_2Ca_{n-1}Cu_nO2n_{+4}$, where $A =$ Bi or Tl, $B =$ Sr or Ba, and $n = 1$ to 4. The compounds in these two systems have identical structures and differ only in atom positions, so it is convenient to deal with their structures together. The highest T_c recorded so far in these systems are 123 K for $n = 3$ in the Tl system, giving $Tl_2Sr_2CaCu_3O_{10}$, also referred to as Tl2223, and 110 K for the structurally similar Bi2223. The toxicity of the Tl oxides has prevented extensive characterization of these compounds as compared to the Bi structures. The crystal structures (Fig. 8) are similar to those of YBCO, but the CuO chain layers are instead replaced by a double layer of TlO. The absence of chains makes the Bi- and Tl-based oxides less susceptible to the stoichiometry of oxygen, though nonstoichiometry is commonly present in these systems due frequently to Ca(Sr) or Cu depletion. The multiplicity of phases is a major problem in the synthesis of homogeneous material in these systems.

The Cu coordination is fivefold square pyramidal with O as for YBCO (Fig. 4). But for $n = 3$, the middle CuO layer contains Cu, which is planar fourfold coordinated. The layer in these systems consists of CuO_2–Ca–CuO_2 layers sandwiched between alkaline-earth-metal oxide B(Sr or Ba)–O layers and by a double layer of A(Tl or Bi)–O. An interesting feature shown by these compounds is the variation of T_c with the number of CuO_2 planes, n. The T_c is found to increase with increasing n, maximizing at $n = 3$. While this confirms the widely accepted fact that the CuO_2 layers play a vital role in superconductivity, for example, the structures with $n = 0$ do not superconduct; increasing the number of layers indefinitely does not necessarily increase T_c.

In addition to these stoichiometric compounds, long sintering times can result in the evaporation of part of an A–O layer, resulting in a monolayer of Tl–O or Bi–O, giving nonstoichiometric oxides. T_c's in the Tl-based compounds vary from 10 K to 121 K depending on the number of copper oxide planes. The family of systems given by the formula $A_2B_2Ca_{n-1}Cu_nO_{2n+4}$ or equivalently by $A_2B_2Ca_nCu_{n+1}O_{2n+6}$ (here n does not correspond to the number of CuO_2 layers) can be extended to other cations such as mercury (Hg), which forms a series of compounds (with A_2 replaced by Hg and B by Ba) with T_c's ranging from 95 K to 133 K, again maximizing for three CuO_2 layers.

Role of Microstructures in High-T_c Superconductors

After the initial excitement and directions towards large-scale technological applications of the HTSC oxides following their discovery in 1986, scientists have realized the difficulty in putting these ceramic oxides to use because they are hard, brittle, and difficult to draw into sheets or wires. The major emphasis in materials science and technology is now on developing the processing and fabrication of thin films for devices. Their novel properties, such as the ability to shield closed volumes from electromagnetic interferences via the Meissner effect, the low microwave surface resistance for use in filters for cellular base stations, the Josephson effect in superconducting quantum interference devices (*SQUIDs*), and the sharp transition in the use of bolometers to detect infrared radiation are in stages of development and use. One exciting application is the use in microelectronics as interconnects—the reduction in Joule heating due to resistanceless current flow will increase the density of devices per chip and the efficiency of packaging. The improvement in RC time constants, increasing the speed of devices, also makes it attractive to consider the integration between superconductors and semiconductors to operate at liquid-nitrogen temperatures. In fact, there are a number of transistors that improve performance when cooled to 77 K.

However, there are a number of problems to be solved—some, such as the magnitude of electric current that HTSC oxides carry and the erratic behavior of weak links in Josephson junctions across grain boundaries, are functions of the Cooper pair coherence length and material quality, while others, such as the degradation on exposure to moisture of YBCO and the formation of ohmic contacts to these oxides, can be solved by proper combination of materials and processing conditions. Thus the material quality or microstructure of thin films seems to be the most important aspect of thin-film study of HTSC superconductors. This leads us to the large influence of grain boundaries on the current-carrying ability of HTSC oxides. While the discussion here pertains directly to YBCO, its extension to other HTSC oxides seems highly likely owing to the central role played by coherence length. As mentioned earlier, the coherence length in oxide superconductors is on the order of a few nanometers, meaning that any imperfection in the material with an influence scaling across dimensions of the same magnitude will break Cooper pairs, mainly because they are formed owing to certain properties exhibited by the perfect crystal structure.

Figure 9 shows an electron micrograph of a grain boundary occurring in a YBCO film with a misorientation between the grains being quite large (28°). It is now well accepted that when the Cooper pairs strike the boundary at an angle, some pass through unbroken, while others break and become nonsuperconducting, resulting in a reduction in the current that emerges on the other side of the boundary. In HTSC terminology, the processes are referred to as pair tunneling and pair breaking, respectively. The grain boundary is said to constitute a *weak link* as a result of this process. Actually, there are two subtle processes involved across boundaries in the HTSC oxides: the weak-link behavior is a result of pair tunneling across an insulating region separating the two superconducting regions or semiconductor–insulator–semiconductor tunneling, as it is referred to, while the other is the proximity effect, and occurs across a metallic or normal boundary, that is, a superconductor–normal conductor–superconductor structure. These two processes have characteristic current–voltage behavior and are easily discernible in classical superconductors where the coherence lengths are large, almost 10 nm to 100 nm. In HTSC oxides, these two processes cannot be differentiated because they occur on length scales of a few nanometers, the same as the coherence length.

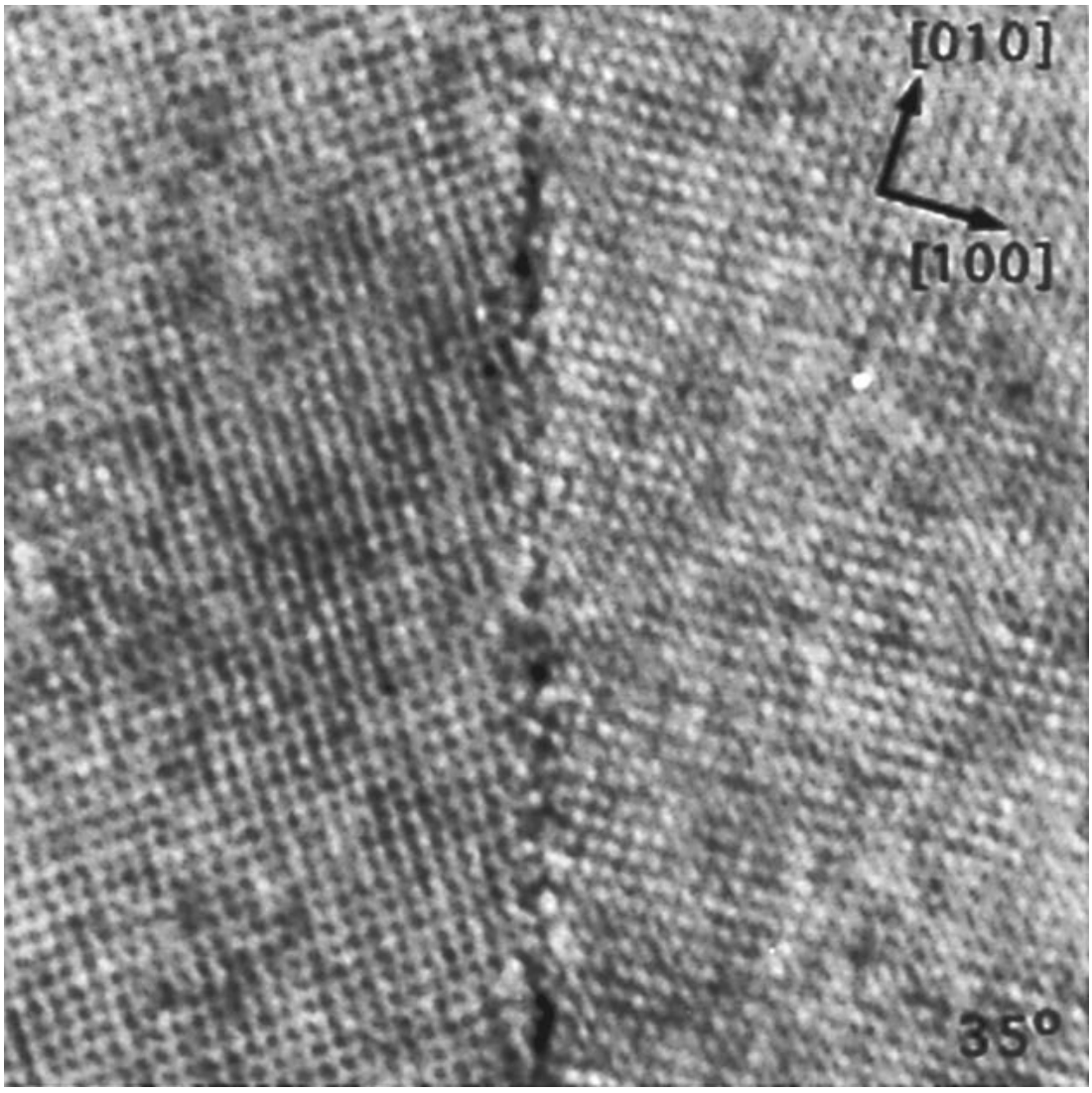

Fig. 9. Large-angle (35°) grain boundary in $Y_1Ba_2Cu_3O_{7-\delta}$. This figure shows a high-resolution TEM image of a typical high-angle pure (001) tilt grain boundary in YBCO.

The significant role of grain boundaries has been emphasized by some lucid experimental demonstrations like those by researchers at IBM (22,23), where they showed that not only does the critical current density (J_c) of the material decrease due to the presence of the boundary, but the J_c also depends on the misorientation angle of the boundary. Figure 10 is a plot of the experimental result of J_c across grain boundaries in YBCO films grown by pulsed laser deposition (*PLD*) (24,25). The plot clearly shows that increasing the misorientation decreases the J_c. This has important implications for devices. High-current-carrying films need boundaries with extremely small misorientations or better still no boundaries at all. To explain the reason for this behavior a number of researchers (23,26,27) have invoked the dislocation structure of low-angle grain boundaries first proposed by Read and Schockley in 1950 (28). Figure 11 demonstrates this idea in a low-angle boundary in a

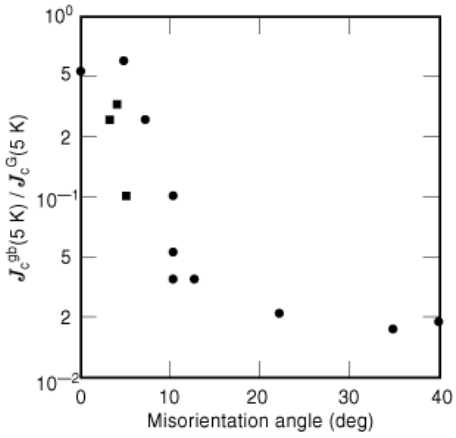

Fig. 10. Experimentally observed variation of the critical current density (J_c) with boundary misorientation (θ). (Adapted Ref. 23.)

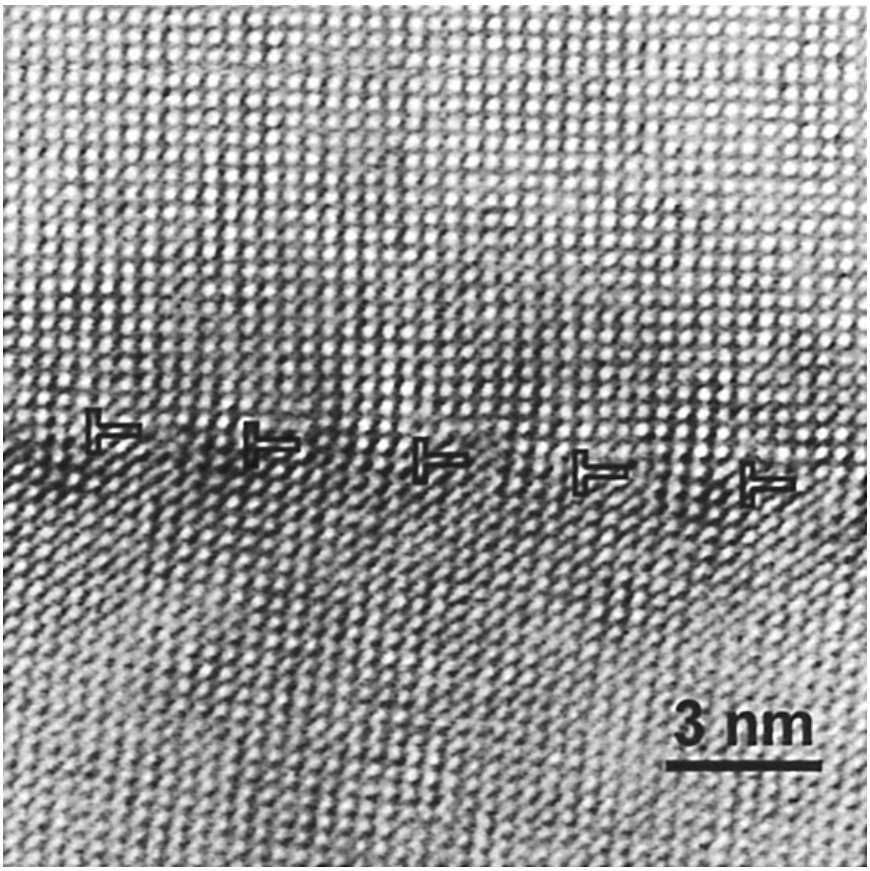

Fig. 11. Low-angle (6°) grain boundary in $Y_1Ba_2Cu_3O_{7-\delta}$ showing the dislocation array. This figure shows a high-resolution TEM image of a low-angle pure (001) tilt boundary in a YBCO film grown by pulsed laser deposition. The boundary misorientation is generated by the equally spaced [100] edge dislocations.

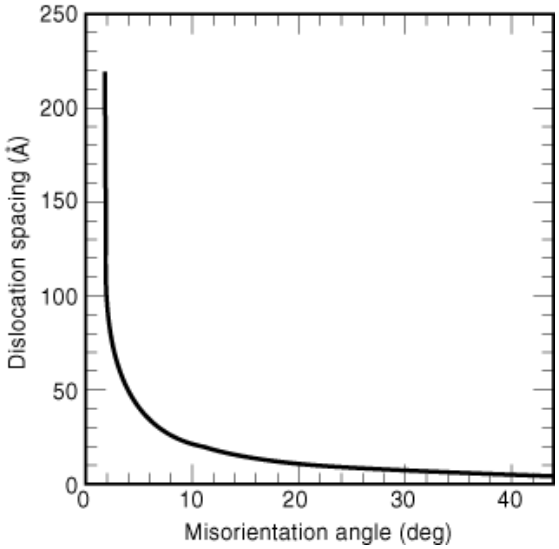

Fig. 12. The variation of dislocation spacing with boundary misorientation (θ). The geometrically calculated variation in spacing parallels the experimental observation of J_c with misorientation shown in Fig. 10.

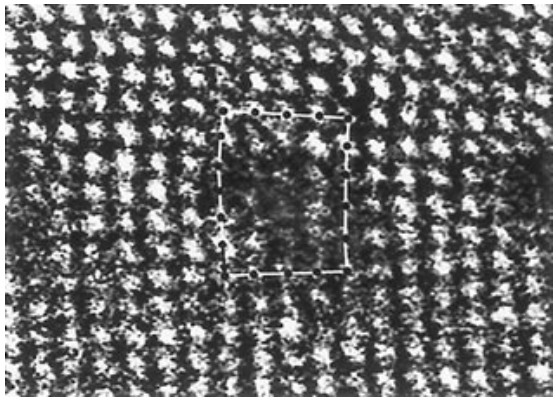

Fig. 13. Dislocation core. This high-resolution TEM image shows the highly distorted structure of the YBCO lattice around a [100] edge dislocation.

YBCO film grown by PLD. The almost regular separation of the dislocations marked in the figure generates the boundary misorientation, and in fact a plot of the dislocation separation versus misorientation (Fig. 12) shows a trend similar to that followed by the J_c in Fig. 10. This similarity was an irresistible attraction to model the current flow as a strong function of the grain-boundary features arising from the dislocation arrays. This includes the finite region along the boundary where the lattice was highly distorted and so superconductivity can be destroyed (29). This is usually observed near or around dislocations like that shown in Fig. 13.

The long-range strain fields are due to the dislocations (30), that distort the crystal structure and affect superconductivity by changing the order parameter (31). The order parameter is the complex quantum-mechanical wave function used to describe the density of Cooper pairs as a function of space, similar to a wave function describing the electron density in a metal, for example, the ability of Cooper pairs to tunnel across

small distortions that are present along the boundary surface due to strains (32). This feature is a function of the boundary width, which describes the region along the boundary in which current flows via tunneling rather than normal current. This parameter is experimentally difficult to observe and various approximations such as the strength of the Burgers vector or via energy minimization (33) are used to calculate it. Another important influence of grain boundaries is the effect of nonstoichiometry commonly observed along the boundary (34), leading to excess charge and subsequently scattering of the Cooper pairs.

Jagannadnam and Narayan have proposed an elegant model to represent the J_c across low-angle boundaries that incorporates all the features mentioned before. While the previous calculations can be done fairly simply, the actual nature of the grain boundaries in HTSC materials needs to be understood fully. It has been shown by various authors that there is a large variation in grain-boundary microstructure even in films prepared under identical conditions (35,36). Recently, it has been seen that even boundaries with a similar misorientation angle along identical crystallographic directions can have different atomic scale structures (37,38).

Compared with strong variation in the low-angle region of 0° to 10° observed in Fig. 10, the J_c in the high-angle region of 10° or more is uniformly low. An early explanation of the IBM group for this saturation effect was the overlapping of dislocations as the boundary misorientation increased. While the notion of the dislocation structure boundaries loses significance at higher angles, it is difficult to even model the current in the high-angle regime for the lack of a uniform description of the boundaries occurring there. Various representations such as the near-coincidence site lattice model (near CSL) or more recently the grain-boundary structure representation in terms of distinct structural units (38,39) are being used to understand the properties of the high-angle boundaries. It has also been difficult to interpret exceptions to the low J_c in high-angle cases, especially for the 90° twist boundary, formed by rotating one unit cell of YBCO 90° with respect to an adjoining cell with the rotation axis being perpendicular to the *c* axis or [001] direction (40,41). Here the absence of the weak-link behavior is a strong suggestion for the fact that high J_c 's are associated with boundaries possessing low energy, also usually accompanied by high symmetry, which is true for the 90° twist boundary. In this light the predominance of asymmetry in grain boundaries in YBCO grown by PLD is an important feature and must be understood more clearly. All these factors lead one to realize that the exact nature of the effect of grain boundaries is far from being fully comprehended and detailed research must be continued for a better understanding.

Role of Substituents in High-T_c Superconductors

The simple copper oxide pervoskites are insulators. By substituting for certain atoms in the unit cell, these materials are made to behave as metals and hence possibly as superconductors. The key characteristic of any superconductor is an energy gap exactly at the Fermi level. Owing to this characteristic, Cooper pairs of electrons do not scatter off the lattice site and break. In the absence of scattering, the propagation of electrons encounters no resistance and the phenomenon of superconductivity is observed. The transition temperature depends strongly on the electronic density of states at the Fermi level. That parameter in turn, is strongly affected by doping of the initial ceramic with other atoms of a different valence to provide extra electrons (or too few electrons, called holes), which are then available for participation in the superconducting mechanism.

The practice of doping has a long history in the field of semiconductors, and chemists have developed great skills in modifying the properties of materials to allow practical electronic devices to be made. It is not surprising to see similar efforts applied to the HTSCs. A tremendous array of substitutions have been tried to improve the mechanical, magnetic, or current-carrying properties of these materials. The complexities of multicomponent phase diagrams prevent some attempted compounds from forming at all. Of those that can be made, either in chemical equilibrium or via a narrow path of kinetics, success is not guaranteed because it is hard to change the electronic properties precisely at the Fermi level. Moreover, the Fermi level is not one single number, but rather there is a Fermi surface in energy space, which is badly distorted from a simple spherical shape by the anisotropy present in the HTSC compounds. Consequently, there is considerable empiricism and guesswork present in any particular choice of chemical substitution in the HTSCs.

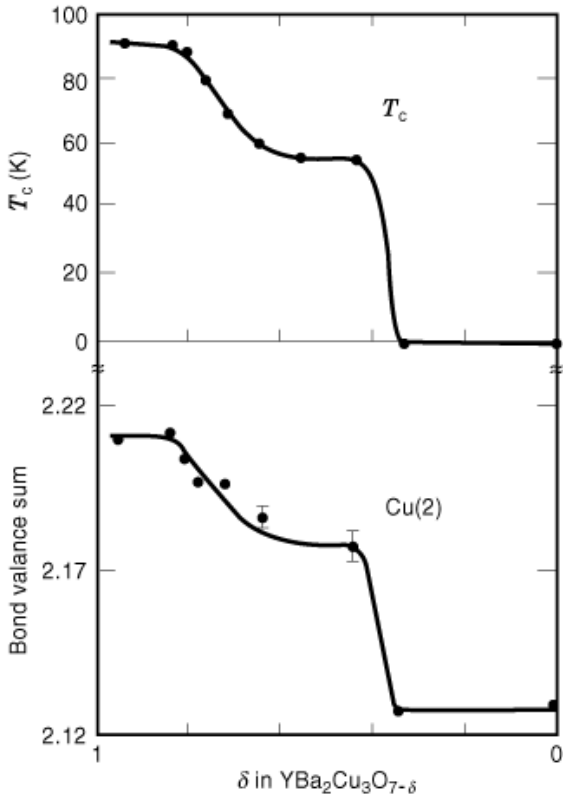

Fig. 14. (a) T_c versus oxygen content in YBCO. (b) Bond valence sum around the copper atom in CuO(2) layer. The purpose of showing the two figures together is to illustrate that T_c is proportional to the oxidation state of the copper atoms in the conduction layer.

Role of Oxygen and Oxygen Vacancies. The role of oxygen in influencing the electronic properties of HTSCs is very crucial. Normally, an oxygen atom takes on two electrons from another atom. Therefore, if it is absent, two more electrons are free to go elsewhere in the crystal. This is how vacancies affect the charge balance in a crystal. The first thing that oxygen vacancies do is change the number of free carriers available in the crystal lattice, which in turn adjusts the Fermi level slightly. The density of states at the Fermi level (N_0) is a key parameter of superconductors: the transition temperature T_c depends on N_0 as $\exp(-1/N_0V)$, where V is the Cooper pairing potential. Small changes in N_0 caused by oxygen vacancies can translate into substantial changes in T_c. It does not take much to change N_0 appreciably. There are about 3.5×10^{13} vacancies/cm^2 in a double-layer compound such as BSCCO, which corresponds to having about 1% of the oxygen atoms missing.

Explaining the role of oxygen vacancies depends upon the charge-transfer model, by which the electrons normally in the CuO_2 planes are transferred to sites elsewhere in the unit cell (42). In YBCO, the oxygen deficiency shows up especially in CuO chains, making their formula $CuO_{1-\delta}$, while the CuO_2 layers remain chemically complete. A key experimental quantity in this model is the oxidation state of copper atoms in the CuO_2 planes. Any deviation from 2.0 indicates that charge transfer is occurring. Because of the mild geometric distortion in the unit cell, the copper–oxygen bonds are stretched slightly in this plane. By measuring the bond lengths around that copper atom, a bond valance sum can be calculated, and this gives the oxidation state (43). As the number of oxygen vacancies varies, both this sum and the superconducting transition temperature T_c vary in the pattern shown in Fig. 14. This presents a very convincing argument for the charge-transfer model.

In TBCCO, there is competition between several different means of causing charge transfer. Those means may be missing metal atoms, extra metal atoms, missing oxygens, extra oxygens, etc. BSCCO exhibits all these conditions, plus the size mismatch between the normal dimensions of the CuO(2) planes and the other planes in the stack is so large that atoms occasionally wind up in the wrong layer. The presence of many slightly different but similar structures in one crystal makes it difficult to interpret experimental data. Nevertheless, despite all the complexity, the average oxidation state for copper is 2.21, which tends to confirm the charge-transfer model.

It should also be noted that an excess of oxygen atoms also acts as a dopant, because it increases the number of sites where electrons can reside, which amounts to creating hole carriers in the crystal. The compound La_2CuO_4 is normally an insulator, but when extra oxygen is forced in, changing it to La_2CuO_{4+d}, it becomes a superconductor. Thus, it appears that a small number of oxygen vacancies offer a way to make small changes in the carrier concentration. Oxygen vacancies are equivalent to the substitution of metal atoms in terms of their effect on the availability of charge carriers.

Role of Substituents in La–(Ba,Sr,Ca)–Cu–O and Nd–Ce–Cu–O Compounds. Substituting for La^{3+} by divalent ions $M = Ba^{2+}$, Sr^{2+}, Ca^{2+} leads to the appearance of metallic conductivity and for $0.05 < x < 0.3$ superconductivity appears in $La_{2-x}M_xCuO_{4-y}$ (LMCO) compounds. $T_c(x)$ is plotted in Fig. 15(a), where the black dots correspond to the appearance of the Meissner signal, and the white dots to its saturated value (44). For larger concentrations of Sr, $x > 0.15$, the oxygen vacancies can appear, $y > 0$; their formation, however, can be suppressed by performing the annealing under high oxygen pressure. Metallic conductivity and superconductivity may also be obtained by increasing the content of oxygen above the stoichiometric value La_2CuO_{4+d}, $d > 0$. In this case, oxygen occupies interstitial positions in layers of La–O. In general, for $La_{2-x}M_xCuO_{4-y}$ one observes the typical dependance $T_c(n)$, which is shown in Fig. 15(b), with x substituted by $n = x-2y$, the number of free charge carriers (holes) per cell in the CuO_2 planes.

Under the substitution of La by the trivalent rare-earth ions RE = Nd, Sm, or Gd, a smooth decrease of T_c with decreasing ionic radius in the series of these ions (45) occurs. At the same time, the value of magnetic moment of RE ion has no effect on T_c, which indicates that the Cooper pairs in the CuO_2 plane are weakly coupled to the magnetic moments of ions in the La–O layers. An analogous situation is observed for electronic superconductors $Nd_{2-x}Ce_xCuO_4$ under the substitution of Nd by the rare-earth ions Pr, Sm, and Eu. The decrease of T_c with decreasing radii of RE ions and primitive cell volume may be related to the decrease of Cu–O bond length.

However, this simple picture contradicts the dependence of T_c on the external pressure. In the La–Sr compounds T_c increases with an increase of pressure, attaining a certain maximum, and even decreases at high pressures. Meanwhile, in Nd–Ce compounds T_c is pressure independent. This difference in the $T_c(p)$ dependence can be related to a special role of apex oxygen: In the tetragonal phase of La–Sr compounds there are two apex oxygens in the complete CuO_6 octahedron, and in the tetragonal phase of Nd–Ce compounds the apex oxygen is absent.

An isovalence substitution of copper by the ions of $3d$ metals has a much stronger effect on T_c. At a concentration of $x = 5\%$ to 7% for Ni and Fe and $x = 2\%$ to 3% for Zn ions, the superconductivity in LMCO disappears (45,46,47). While the disruption of superconductivity due to scattering of the Cooper pairs on magnetic impurities is well known, the suppression of T_c due to Zn impurities in CuO planes is characteristic of copper-oxide superconductors. Figure 16 shows the $T_c(x)$ dependence for the Zn impurity in $La_{2-x}Sr_xCuO_{4-y}$ LSCO and YBCO (47). It is possible that Zn ions, which have a filled $3d$ shell ($3d^{10}$), destroy a rather complicated correlation conduction band in CuO_2 planes that is related to Cu–O charge transfer as shown in Fig. 17 (48). This leads to suppression of superconductivity. In this context, one can consider Zn^{2+} ions as effective magnetic scatterers, because they substitute Cu^{2+} ions, which have a local magnetic moment.

Role of Substituents in YBCO Compounds. A large number of studies have been carried out to investigate the role of constituents in YBCO compounds. Immediately after superconductivity with $T_c = 90$ K in the YBCO system was observed, a large class of RBCO compounds with a similar T_c was prepared. This

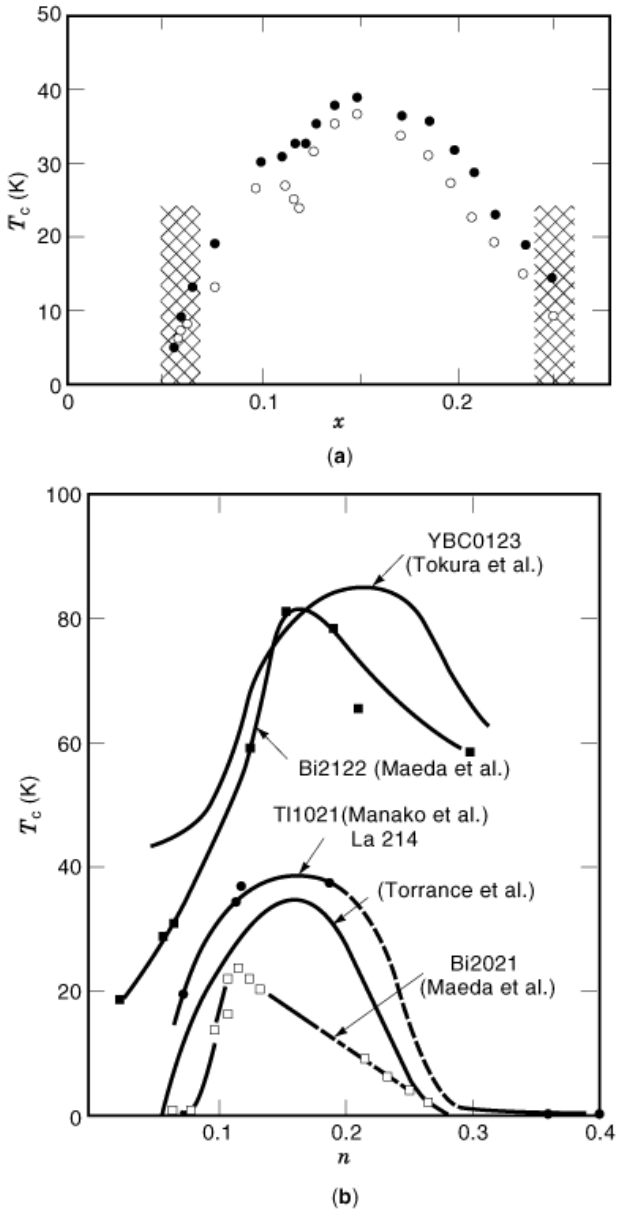

Fig. 15. (a) T_c as a function of Sr concentration in ($La_{1-x}S_{rx})_2CuO_4$ [5.13] and the general dependence $T_c(n)$ on the concentration of holes n in the CuO_2 planes for some copper-oxide superconductors. (After Tiokura, 1992.)

was done by substituting Y by lanthanides Ln = La, Nd, Sm, Eu, Gd, Dy, Ho, Er, Tm, Yb, or Lu. For these no separation of T_c in the compounds with rare-earth ions having a large magnetic moment has been observed. This indicates their weak coupling with the in-plane holes. The exceptions are Ce and Er ions, whose formal valence is +4, which violates the isovalence of the substitution of Y ions and can change the concentration of carriers in CuO_2 planes. In order to investigate this concept, the system $(Y_{1-x-y}Ca_y)\ Prx_{Ba2}Cu_3O_{7-\delta}$ has

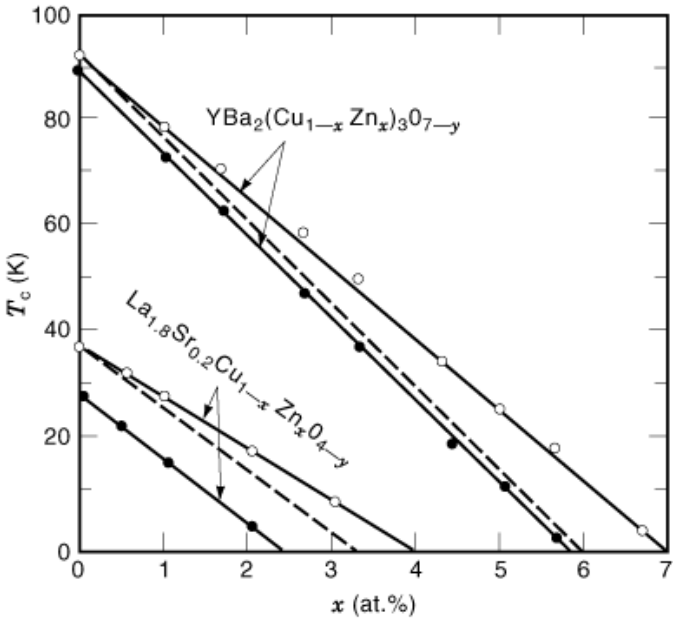

Fig. 16. T_c as a function of impurity x in a $La_{1.8}Sr_{0.2}Cu_{1-x}Z_{nx}O_{4-y}$ compound. For comparison the variation of T_c in $YBa_2Cu_{1-x}Z_{nx}O_{7-\delta}$ is also shown as a function of x.

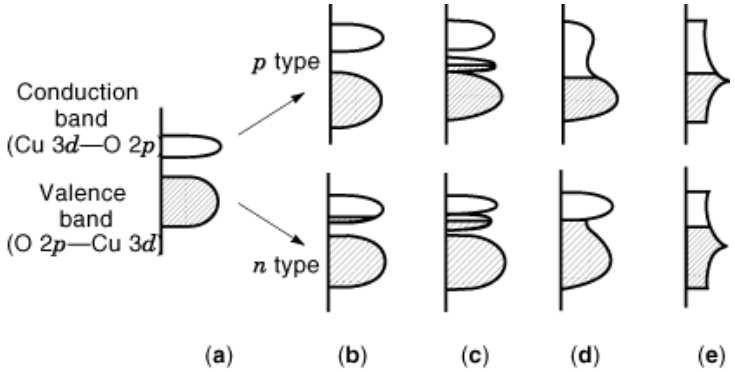

Fig. 17. Schematic of electronic structure of copper oxide superconductors accounting for (a) the correlation splitting of a $pd\sigma$ band, and some models for its change upon p or n doping: (b) rigid band, (c) impurity band, (d) filled gap, and (e) local density approximation. [48]

been examined (49). The $T_c(y)$ dependence for different x and $T_c(x)$ at $y = 0$ is shown in Figs. 18(a) and 18(b), respectively. The substitution of Pr^{4+} for Y decreases the number of in-plane holes, whereas substitution of Ca^{2+} has the opposite effect. This allows one to investigate separately the dependence of T_c on the concentration of holes $n\ \alpha\ (y-x)$ and on the magnetic scattering on the localized moments of Pr. Indeed, it follows from Fig. 18(a) that $T_c(y)$ has a typical hole dependence with a maximum at an optimal concentration of holes n for various concentrations x of Pr ions. The location of these maxima shifts to larger values of y with an increase of Pr content, which proves directly that the concentration of carriers $n\ \alpha\ (y-x)$ decreases with an increase of x. At the same time, a decrease of the maximum value of $T_c(x,y)$ for the optimal n is observed, which indicates

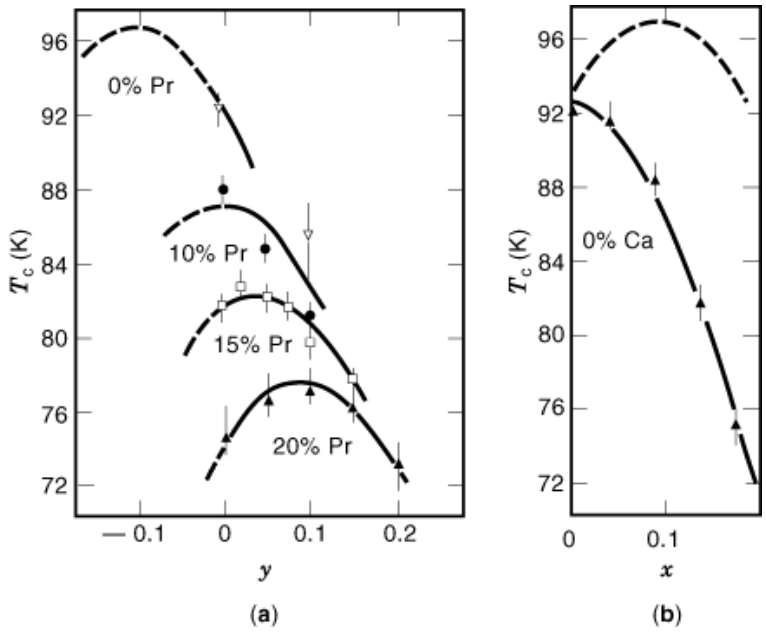

Fig. 18. The dependence of T_c in $Y_{1-x-y}Ca_yPr_xBa_2Cu_3O_{6.95}$ (a) on the concentration of Ca at a fixed content of Pr and (b) on the concentration of Pr for $y = 0$. The dotted line is the T_c dependence on the concentration of holes without magnetic scattering. [After Neumeier et al. 49]

a decrease of T_c due to magnetic scattering leading to the destruction of Cooper pairs. Figure 18(b) shows the effect of a change of the number of carriers on $Tc(x,y = 0)$. One can see that the maximum value of T_c in YBCO at $7-\delta = 6.95$ is attained under a small decrease of the number of in-plane holes due to the tetravalent impurities. In the course of investigations of the effect of impurity substitution on T_c, one must control the content of oxygen as it influences the number of carriers in CuO_2 planes and determines the value of T_c.

An investigation of the effect of substitution of Ba in YBCO by the rare-earth ions has been carried out for the $Ln(Ba_{2-x}L_{nx})Cu_3O_{7-\delta}$ compounds, where Ln = La, Nd, Sm, Eu, Gd. All the lanthanides produce an equal decrease in T_c with respect to the concentration of impurities x. This indicates a weak sensitivity of the superconducting transition to the appearance of magnetic moments on the Ba sites. A phase transition is also observed from orthorhombic to tetragonal (at $x = 0.2$ to 0.3), which, however, did not have significant effect on the superconducting properties. In view of an often uncontrolled increase of oxygen content $7 - \delta > 7$ under the substitution of Ln for Ba and a complicated rearrangement of charge in the layers Ba–O(4), Cu(1)–O, Cu(2)–O(2,3), it is not possible to unambiguously conclude regarding the dependence of T_c on the concentration of holes in CuO_2 planes.

In the YBCO compounds a more complicated effect of the substitution for copper ions has been observed. The complicated effect arises due to two reasons. First, in YBCO compounds there are two nonequivalent copper positions, whose substitution has a different effect on their electronic structure and superconductivity. Second, some impurities such as Fe and Co affect the oxygen content and the short-range order in Cu(1)–O(1) layer, which may change the number of carriers in the Cu(2)–O(2,3) planes.

It is interesting to study the effect of substituting Cu by ions of $3d$ elements M^{2+} = Ti($3d^2$), Cr($3d^4$), Mn($3d^5$), Fe($3d^6$), Co($3d^7$), Ni($3d^8$), and Zn($3d^{10}$). It has been observed that for $x = 0.1$ in $YBa_2(Cu_{1-x}M_x)_3O_{7-\delta}$ the strongest suppression of T_c occurs for the ions of Fe and Co, having the maximum magnetic moment, and also for the Zn ions (50). However, some investigations have demonstrated that in case of Fe and Co an extra

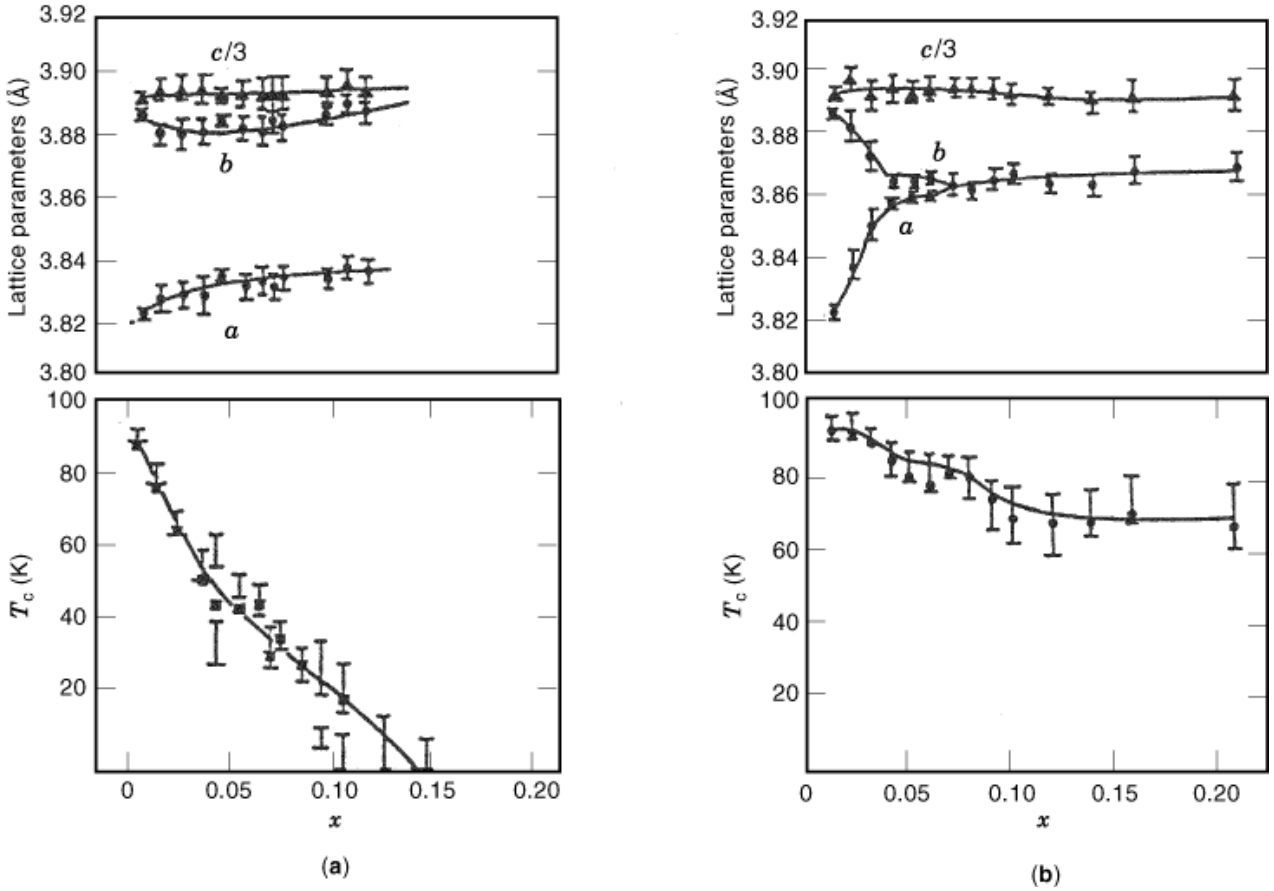

Fig. 19. The dependence of lattice parameters and T_c on the concentration of impurities in $YBa_2(Cu_{1-x}M_x)O_{7-\delta}$ for (a) Zn, and (b) Ga.

annealing in an oxygen atmosphere restores the value of T_c for x less than or equal to 0.35 almost completely, but does not relax the decrease of T_c by the impurities of Zn and Ni (51). Such different effects of annealing on T_c in impurity compounds of YBCO is explained by the fact that at low concentrations the ions of Co and Fe preferentially occupy the position of Cu(1), and the ions of Zn and Ni the position of Cu(2). Therefore, annealing in oxygen restores the oxygen content and its coordination in the Cu(1)–O(1) layer for the Co and Fe impurities, but has no effect on the plane Cu(2)–O(2,3) for the Zn and Ni impurities.

A more detailed analysis of the effect of diamagnetic impurities under a substitution for copper is also available in literature (52). In that study $Zn^{2+}(3d^{10})$ and $Ga^{3+}(3d^{10})$ impurities were used. Their ionic radii for a filled$3d$ shell, $R(Zn^{2+}) = 0.75$ Å, $R(Ga^{3+}) = 0.62$ Å are close to $R(Cu^{2+}) = 0.73$ Å, which allows one to obtain single-phase samples in a wide range of impurity concentrations. Neutron diffraction measurements have indicated that Zn primarily occupies the position of Cu(2), and Ga the chain positions of Cu(1). The dependence of T_c and lattice constants are shown in Fig. 19(a) for Zn and Fig. 19(b) for Ga. Zn impurities in the layers Cu(2)–O(2,3) have only a small effect on the parameters of the lattice, preserving the orthorhombic phase, but lead to a rapid suppression of T_c. The oxygen content remains close to optimal (6.8 and 7.0 for samples with Zn and Ga, respectively), and therefore the transition to the tetragonal phase in the case of Ga is not related

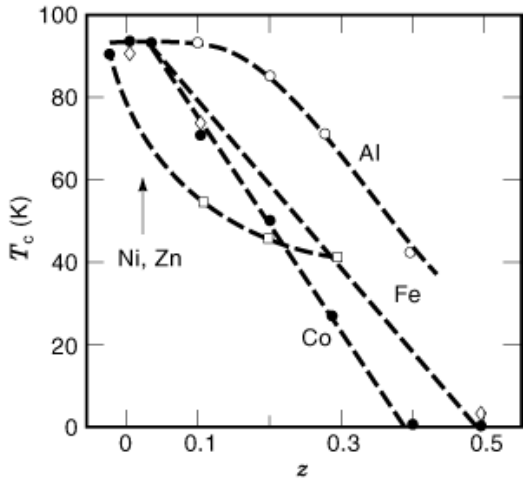

Fig. 20. T_c versus the concentration of impurities $M = Ni^{2+}$ and Zn^{2+} and $M = Al^{3+}$, Fe^{3+} and Co^{3+} in $YBa_2Cu_{3-z}M_zO_{7-\delta}$. [After Taraskon et al. 53

to the deficiency of oxygen. The resistance $\rho(x)$ in the normal phase increases much faster for Ga impurities than that for Zn, while they have the converse $T_c(x)$ dependence. These experiments clearly demonstrate that the main role in the appearance of superconductivity in copper-oxide compounds is played by the CuO_2 planes, where the specific properties of copper in $3d^9$ states are necessary to attain high T_c.

According to studies of structural, magnetic and superconducting properties of $YBa_2Cu_{3-z}M_zO_{7-\delta}$ compounds, paramagnetic and diamagnetic impurities affect these properties differently (49). Here M = Ni,Fe,Co represent paramagnetic impurities and M = Zn,Al represent diamagnetic impurities. It has been observed that the divalent impurities Zn^{2+} and Ni^{2+} do not change the content in the sample and, when occupying positions in CuO_2 planes, preserve the orthorhombic phase in the domain of single-phase states (for $z \leq 0.3$ or the concentration $x = z/3 < 0.1$). Al^{3+} impurities as well as Co and Fe being in the trivalent state occupy the chain Cu(1) positions. They lead to an increase of oxygen content, filling the vacancies near the impurity site and leading to a transition to the tetragonal phase for $z < 0.1$. The dependence of $T_c(z)$ for these impurity substitutions is shown in Fig. 20. It is clear from this figure that substituting in-plane Cu(2) by Zn impurities leads to a rapid decrease of T_c while substituting the in-chain Cu(1) by trivalent impurities Al, Fe, Co has a much weaker effect on T_c. Apparently, both substitution of impurities for in-chain Cu(1) and changing the oxygen content have the same effect on the charge transfer from the chains to the planes, causing the transition from insulating to metallic phase which becomes superconducting. Note that in a series of experiments a more complicated dependence of T_c on the concentration of impurities that substitute for copper in YBCO compounds has also been observed (54,55).

There are certain elements in the periodic table that have been shown to be unreactive with YBCO materials (56,57). When such elements are added to YBCO compound, they do not substitute any of the elements in the lattice and tend to reside in intergranular regions (58). However, they have been found to affect significantly the superconducting properties of the YBCO material by modifying the grain-boundary properties. Silver is one such element that has most widely been used as a dopant to modify the grain-boundary properties of YBCO system (59). Shown in Fig. 21 is the variation of T_c and J_c of YBCO films doped with different amount of silver. All the films were deposited in situ on (100)$LaAlO_3$ substrates using a pulsed laser deposition techniques. Different levels of doping in YBCO films were obtained by using targets containing different concentration of silver metal. Figure 21 shows that there is a one-to-one correlation between the resistivity and critical current

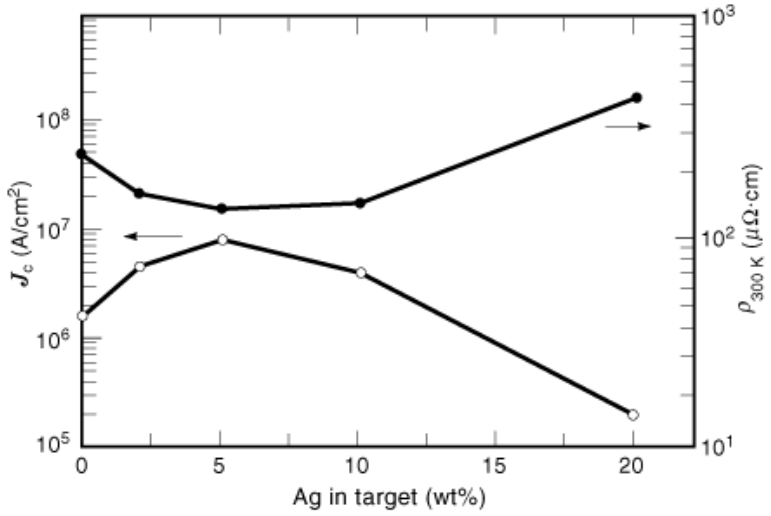

Fig. 21. Variation of room-temperature resistivity and critical current density (J_c) at 77 K of films obtained from YBCO targets having different dopant level of Ag. [After Kumar et al. (58)

densities. This correlation is due to weak-link coupling in which the critical current density of weak links should increase with lowered resistivity (60). Figure 21 also shows that films made using targets having 5% of silver gives highest J_c and the lowest room-temperature resistivity. This can be explained on the basis of the fact that a lower percentage of silver in the target may not be able to provide sufficient silver atoms required to enhance grain growth and liberate oxygen at the periphery of the grains of films, whereas a higher percentage of silver in the target would result in higher doping of YBCO films. Higher levels of silver in the targets and films may give rise to the formation of some impurity phases. According to Kao et al. (61), it is also possible that beyond the optimum Ag content, Ag atoms may enter the CuO basal panes in the orthorhombic structure and cause deterioration in T_c and J_c of the sample.

Since the grains in the superconducting films are coupled to each other through the materials in the grain boundaries, the presence of silver in the grain boundaries affects the properties of YBCO materials very significantly. The materials in the boundaries are the rejects of the grains, and they may be either metallic or insulating in nature. Depending upon the nature of the material in the grain boundary, the couplings are known as S–I–S (60) or S–N–S (62,63) where S, I, and N stand for superconductor, insulator, and normal metal, respectively. The temperature dependence of the critical current density as a function of temperature gives an idea of the nature of the weak links present in superconducting samples with different amount of grain-boundary dopants (60). If the superconducting grains are coupled to each other by an insulating phase in the grain-boundary region, the current density of such junctions is determined by the expression suggested by Ambegoakar and Baratoff (60),

$$J_c(T) = \pi \Delta(T)/2eR_N \tanh[\Delta(T)/2k_BT] \qquad (1)$$

where R_n is junction resistance and $\Delta(T)$ is energy gap. When T is close to T_c,

$$J_c(T) \propto (1 - T/T_c) \qquad (2)$$

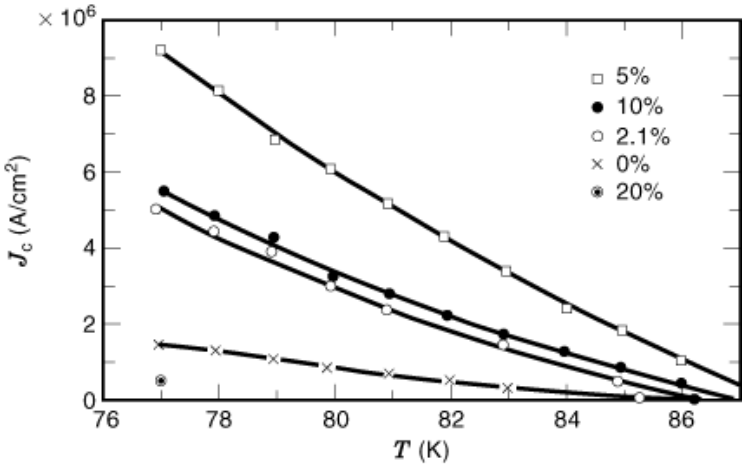

Fig. 22. Critical current density versus temperature plots for undoped and Ag-doped YBCO films on $LaAlO_3$ substrates grown under identical conditions. [After Kumar et al. (1994).]

If the suppression of the order parameter is taken into account, calculation through Ginzberg–Landau theory gives the following $J_c(T)$ relation for an S–I–S network (64):

$$J_c(T) \propto (1 - T/T_c)^{3/2} \tag{3}$$

However, if the superconducting grains are coupled to each other by normal-metal type material in the grain-boundary region, the junctions are known as S–N–S junctions and the current density of such junctions is given by the expression suggested by de Gennes (62) and Clarke (63),

$$J_c(T) = J_{c0}(1 - T/T_c)^2 e^{-d/\xi_N} \tag{4}$$

where d is the thickness of the grain boundary layer and ξ_n is the normal-metal coherence length. Ignoring the weak temperature dependance of ξ_n compared to the $(1 - T/T_c)^2$ term, we obtain

$$J_c(T) \propto (1 - T/T_c)^2 e^{-d/\xi_N} \tag{5}$$

or

$$\sqrt{J_c(T)} \propto J_{c0}(1 - T/T_c) e^{-d/2\xi_N} \tag{6}$$

The value of the slope of the J_c versus $T_c - T$ plot can be used as a figure of merit of the film, since the larger the slope of the plot the better the quality of the film. Having identified the nature of the weak link from the J_c versus $T_c - T$ plot, one can derive other useful information from this plot regarding the width of the grain boundary in different films. From Eq. (6) it is obvious that the slope of the J_c versus $T_c - T$ plot is proportional to the inverse exponent of the width of the grain boundary d. This concept was used by Kumar et al. (65) to understand the reason for the difference in critical current densities of undoped and Ag-doped films. They fabricated a series of YBCO films with different concentration of Ag. Plots of the temperature dependance of the critical current density of these films are shown in Fig. 22. Determining the values of J_c and $T_c - T$

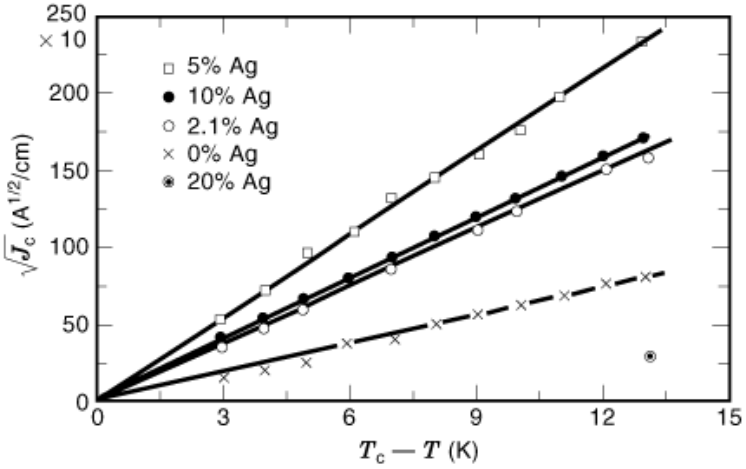

Fig. 23. J_c versus $T_c - T$ plots of undoped and Ag-doped YBCO films on $LaAlO_3$ substrates grown under identical conditions. [After Kumar et al. 65]

from Fig. 22, the J_c versus $T_c - T$ plots of undoped and Ag-doped YBCO films were obtained and are shown in Fig. 23. It is clear from this figure that both undoped and Ag-doped YBCO films follow the S–N–S model, but their grain-boundary widths are different. The variation in grain-boundary widths in undoped and Ag-doped films is as follows: $d_{0\%}$:$d_{2\%}$:$d_{5\%}$:$d_{10\%}$:$d_{20\%}$ :: 1.0:0.6:0.5:0.65:2.0. Owing to differences in grain-boundary width, the grain-boundary resistance and hence the strength of S–N–S coupling in these films are also different. In the present example, the coupling is maximum in the case of 5 wt % Ag-doped film and is minimum in the case of 20 wt % Ag-doped film, and therefore the former has the maximum current density and the latter has the least.

Role of Substituents in Bi-, Tl-, and Hg-Based Compounds. The copper superconductors containing layers of bismuth oxide, thallium oxide, or mercury oxide exhibit superconductivity at higher transition temperatures than YBCO. Because all three types of compounds have very similar structures, it is convenient to discuss the role of dopants in these compounds together. Among the bismuth-oxide-based superconductors, the structures of greatest interest are $Bi_1Sr_2Ca_1Cu_2O_{10}$ (BSCCO-1212) and $Bi_2Sr_2Ca_2Cu_3O_{10}$ (BSCCO-2223). The most familiar substitution in bismuth-oxide-based superconductors is to replace bismuth with lead. This has relatively minor effects on the superconducting properties, but it strongly affects the kinetics and phase equilibrium of the mixture. The result is that $(Pb,Bi)_2Sr_2Ca_2Cu_3O_{10}$ is much easier to make than BSCCO-2223 without lead. In a similar analogy with the rare-earth substitutions in YBCO, the partial replacement of Bi with Pb makes little difference electronically, and thus changes the T_c only very modestly.

In both the thallium- and bismuth-based superconductors, the strategy of doping is driven by the conjectures of each investigators about what will produce desired properties. The number of substitutions possible on those unit cells, together with the complexity of their phase diagrams, requires verification of hypotheses by empirical means. The familiar series of thallium superconductors are made of Tl, Ba, Ca, Cu, and O. The transition temperatures of various phases are generally above 100 K. A less well-known series is based on Tl-Sr-Ca-Cu-O (TSCCO) with Sr playing the equivalent role of Ba. TSCCO is nonsuperconducting. Sheng et al. (66) have shown that the substitution of the trivalent Y for the divalent Ca brings an extra electron onto that layer in the unit cell, leading to the conversion of material to the superconducting phase with a T_c of 80 K. The goal of most substitutions is to change the number of carriers (holes, usually) by doping the various layers of the unit cell. As in YBCO compounds, the carrier concentration can be manipulated to optimize T_c by doping with elements of different valance. Using this concept a T_c of 110 K has been achieved in TSCCO by

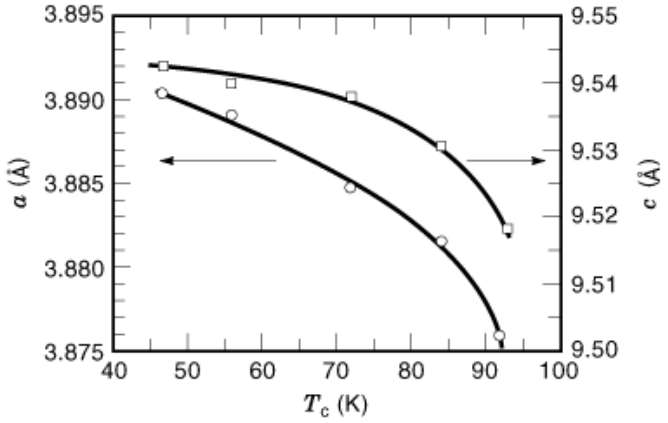

Fig. 24. Lattice parameters a and c versus T, for $HgBa_2CuO_x$, samples with different oxygen contents. [After Wagner et al. (70).]

combining the lead–bismuth substitution for thallium with a substitution of yttrium for calcium (67,68). The chemical formula is typically $(Tl_{1-x}M_c)Sr_2(Ca_{1-h}Y_h)Cu_2O_{7-\delta}$, with various choices of x and h between 0 and 1, and δ around 0.1. The T_c of this series has been found to lie between 40 K and 100 K.

The first mercury-based HTSC is $HgBa_2CuO_{4+\delta}$ (69). As in the case of $La_2CuO_{4+\delta}$, the primary doping mechanism is an interstitial oxygen. The maximum $T_c = 95$ K when δ is approximately equal to 0.06, but drops to 59 K when $\delta = 0.01$. The change in oxygen content changes the unit-cell a and c dimensions. The associated change in T_c correlates with these dimensions as shown in Fig. 24 (70). Experiments have shown that about 8% of copper occasionally substitutes on the mercury site, but a systematic pattern of changes in T_c is yet to be established. The new sister compounds with two or three CuO_2 layers that have $T_c = 133$ K also contain a slight excess of oxygen (6). It is expected that the effect of oxygen interstitial and vacancies may be similar to that found in previous HTSCs.

Conclusion

This article deals with the structure and role of constituents in high-temperature superconductors. After introducing certain basic terminology, we have presented schematic drawings of the unit cells of several different high-temperature superconductors. The high-temperature superconductors have in common the presence of copper-oxide layers, with superconductivity taking place between these layers. The unit cells are not perfectly symmetric, which has important consequences for superconductivity. For the role of substituents, the range of possible substitution in high-T_c superconductors is enormous. This article presented some examples with an effort to explain why researchers preferentially try particular kinds of doping. The motivation is to manipulate the interacting electrons so as to learn more about the metallic state of the ceramic oxides. The goal of doping research is not to raise T_c through empiricism but to establish an experimental foundation on which a theory can be built to explain the mechanism of high-T_c superconductors.

BIBLIOGRAPHY

1. H. K. Onnes, Report on the research made in the Leiden Cryogenic Laboratory between the *2nd and 3rd Int. Congr. on Refrigeration*, Suppl. No. 34b, 1913.
2. J. G. Bednorz K. A. Muller, *Z. Phys. B*, **64**: 189, 1986.

3. X. D. Wu, *et al.Appl. Phys. Lett.*, **51**: 861, 1987.
4. H. Maeda, *et al.Jpn. J. Appl. Phys.*, **27**: L2, 1998.
5. Z. Z. Sheng A. M. Hermann, *Nature*, **332**: 138, 1988.
6. A. Schilling, *et al. Nature*, **363**: 56, 1993.
7. M. Nunez-Reguerio, *Science*, **262**: 97, 1993.
8. C. W. Chu, *Nature*, **365**: 323, 1993.
9. L. N. Cooper, *Phys. Rev.*, **104**: 1189, 1956.
10. F. London H. London, *Proc. R. Soc. London, Ser, A.*, **149**: 7, 1935.
11. J. C. Phillips, in *Physics of High-T, Superconductors*, New York: Academic Press, 1989.
12. A. Wattiaux, *et al. C. R. Seances Acad. Sci.*, **310**: 1047, 1990.
13. C. W. Chu, *et al. Phys. Rev. Lett.*, **58**: 405, 1987.
14. J. Fonteuberta, L. Fabrega, A. V. Narlikar (ed.), *Studies in High Temperature Superconductors*, vol. 16, New York: Nova Science, 1996.
15. D. Jerome, W. Kang, S. S. P. Parkin, *J. Appl. Phys.*, **63**: 4005, 1988.
16. J. M. Tranquada, *et al. Phys. Rev. B*, **38**: 8893, 1988.
17. D. Kumar, Electrical, structural and chemical properties of laser ablated YBCO thin film, Ph.D. thesis, Indian Institute of Technology, Bombay, 1993.
18. S. J. Rothman, *et al. Proc. DIMETA-88, Int. Conf. Diffus. Met. Alloys*, Hungary, 1988.
19. R. J. Cava, *Nature*, **338**: 328, 1989.
20. T. Siegrist, *et al. Nature*, **334**: 231, 1988.
21. C. C. Torardi, *et al. Science*, **240**: 631, 1988.
22. P. Chaudhari, *et al. Phys. Rev. Lett.*, **60**: 1653, 1988.
23. D. Dimos, P. Chaudhari, J. Mannhart, *Phys. Rev. B*, **41**: 4038, 1990.
24. J. Narayan, *et al. Appl. Phys. Lett.*, **51**: 1845, 1987.
25. D. Dijkkamp, *et al. Appl. Phys. Lett.*, **51**: 619, 1987.
26. D. Dimos, *et al. Phys. Rev. Lett.*, **61**: 219, 1988.
27. K. Jagannadham J. Narayan, *Philos. Mag.*, **59**: 917, 1989.
28. W. T. Read W. Shockley, *Phys. Rev.*, **78**: 275, 1950.
29. K. Jagannadham J. Narayan, H. S. Kwok (ed.), *Superconductivity and Applications*, New York: AIP, pp. 37–49.
30. M. F. Chisholm S. J. Pennycook, *Nature*, **351**: 47, 1991.
31. V. L. Ginzberg L. D. Landau, *Zh. Eksp. Teor, Fiz.*, **20**: 1064, 1950.
32. G. Deutsher, *Physica C*, **153-155**: 15, 1988.
33. K. Jagannadham J. Narayan, *Mater. Sci. Eng. B*, **8**: 5, 1991.
34. N. D. Browning, *et al. Physica C*, **212**: 185, 1993.
35. S. McKernan, M. G. Norton, C. B. Carter, *J. Mater. Res.*, **7**: 1052, 1992.
36. D. M. Kroeger, *et al. J. Appl. Phys.*, **64**: 331, 1988.
37. S. Oktyabrsky, *et al. Proc. Microse. Microanal.*, 4, 1998.
38. R. Kalyanaraman, *et al. Mater. Res. Soc. Proc.*, **526**: in press.
39. M. M. McGibbon, *Philos. Mag. A*, **73**: 625, 1996.
40. S. E. Babcock, *et al. Nature*, **347**: 167, 1990.
41. C. B. Eom, *et al. Science*, **251**: 780, 1991.
42. J. D. Jorgensen, *et al. Phys. Today*, **44**: 34, 1991.
43. J. D. Jorgensen, *et al. Phys. Rev. B*, **36**: 3608, 1987.
44. H. Takagi, *et al. Phys. Rev. B*, **40**: 2254, 1989.
45. L. H. Greene B. G. Bagley, D. M. Ginsberg (ed.), *Physical Properties of High-Temperature Superconductors*, vol. 2, Singapore: World Scientific, 1990, p. 509.
46. J. T. Markert, Y. Dalichaouch, M. B. Maple, D. M. Ginsberg (ed.), *Physical Properties of High-Temperature Superconductors*, vol. 1, Singapore: World Scientific, 1989, p. 509.
47. A. V. Narlikar, C. V. N. Rao, S. K. Agarwal, A. V. Narlikar (ed.), *Studies of High Temperature Superconductors*, vol. 1, New York: Nova Science, 1989, p. 341.
48. J. Fink, *et al. Proc. Int. Semin High T_c. Supercond.*, Dubna, JINR E17-90-472, 1990, p. 8.
49. J. J. Neumeier et al., *Phys. Rev. Lett.*, **63**: 2516, 1989.

50. G. Xiao, *et al. Phys. Rev. B*, **35**: 8782.
51. Y. Oda, *et al. J. Phys. Soc. Jpn.*, **57**: 4079, 1988.
52. G. Xiao, *et al. Phys. Rev. Lett.* **60**: 1446, 1988.
53. J.-M. Taraskon, *et al. Phys. Rev. B*, **37**: 7458, 1988.
54. A. M. Balagarov, J. Piechota, A. Pajaczkowska, *Solid State Commun.*, **78**: 407, 1991.
55. S. Katsuyama, Y. Ueda, K. Kosuge, *Mater. Res. Bull.*, **24**: 603, 1989.
56. Williams Chaudhary, 1988.
57. Kubaschewki Alcock, 1979.
58. D. Kumar, *et al. Appl. Lett.*, **62**: 3522, 1993.
59. J. Joo, *et al. Appl. Supercond.*, **2**: 401, 1994.
60. V. Ambegaoakar A. Baratoff, *Phys. Rev. Lett.*, **10**: 486, 1963.
61. Y. H. Kao, *et al. Appl. Phys. Lett.*, **67**: 353, 1990.
62. P. G. de Gennes, *Rev. Mod. Phys.*, **36**: 225, 1964.
63. J. Clarke, *Proc. R. Soc. London, Ser. A*, **308**: 447, 1969.
64. M. Tinkham, in *Introduction to Superconductivity*, New York: McGraw-Hill, 1975.
65. D. Kumar, P. R. Apte, R. Pint, *J. Appl. Phys.*, **77**: 5802, 1995.
66. J. P. Sheng, *et al. Appl. Phys. Lett.*, **54**: 280, 1989.
67. R. S. Liu, *et al. Appl. Phys. Lett.*, **57**: 2492, 1988.
68. R. S. Liu, *et al. Physica C*, **159**: 385, 1989.
69. S. N. Putalin, *et al. Nature*, **362**: 226, 1993.
70. J. L. Wagner, *et al. Physica C*, **210**: 447, 1993.

READING LIST

IEEE Trans. Electron. Dev., **34**, 1987, special issue.
Y. Jeon, G. Liang, J. Chen, M. Croft, M. W. Ruckman, D. Di Marizo, M. S. Hegde, (1990), *Phys. Rev. B*, **41**, 4066.
W. Jin, M. H. Dagani, R. K. Kalia, P. Vashishta, *Phys. Rev. B*, **45**, 5535.
D. Kumar, (1994) in Electrical, Structural and Chemical Properties of Laser Ablated YBCO Thin Films, Ph. D. Thesis (Indian Institute of Technology, Bombay, India).
G. Xiao, Cieplak, D. Musser, M. Z., A. Gavrin, F. H. Streitz, A. Bakhshai, C. L. Chien, J. J. Rhyne, J. A. Gotaas, (1988), *Nature*, **332**, 238.

D KUMAR
RAJIV K. SINGH
R. KALYANARAMAN
S. OKTYABRSKY
K. JAGANNADNAM
University of Florida
J. NARAYAN
North Carolina State University